Analysis Of Real-Life Multi-Input Loading Histories For The Reliable Design Of Vehicle Chassis

Emilien Baroux, Benoit Delattre, Andrei Constantinescu, Patrick Pamphile, Ida Raoult

Version of Record: https://www.sciencedirect.com/science/article/pii/S2452321622002633
Manuscript_7e954758d3689883c4872b15ecba6169

Available online at www.sciencedirect.com

ScienceDirect

Structural Integrity Procedia 00 (2021) 1–??

Journal Logo

www.elsevier.com/locate/procedia

Fatigue Design 2021, 9th Edition of the International Conference on Fatigue Design

Analysis Of Real-Life Multi-Input Loading Histories For The Reliable Design Of Vehicle Chassis

Emilien Baroux[a,b,c,d,*], Benoit Delattre[a], Andrei Constantinescu[b], Patrick Pamphile[c,d], Ida Raoult[a]

[a] *Stellantis, Technical Center Vélizy, Route de Gisy, 78140 Vélizy-Villacoublay, France*
[b] *Laboratoire de Mécanique des Solides, Institut Polytechnique de Paris, Ecole Polytechnique, 91120 Palaiseau, France*
[c] *Laboratoire de Mathématiques d'Orsay, Université Paris-Saclay, Bat 407, 91405 Orsay Cedex 9, France*
[d] *CELESTE team Inria-Saclay, 1 Rue Honoré d'Estienne d'Orves, 91120 Palaiseau, France*

Abstract

In order to reliably design automotive structures, engineers need to determine and justify validation conditions and levels. These must stem from a thorough knowledge of structural damage induced by service loading conditions. From multi-input variable amplitude loading histories applied on a car's wheel axles, we propose a multidimensional pseudo-damage description for the design of car chassis weak points. We present a multivariate description of client loading histories. We use it in a statistical analysis of a labelled measurement campaign to explain the heterogeneity of car driver profiles. Finally, we explore the question of complex load damage reconstruction using proving ground reference loads.

Keywords: Automotive fatigue design, Multi-input variable amplitude loads, Multiaxial fatigue, Structural damage, Multivariate analysis, Statistical learning, Loading reconstruction

1. Introduction

Ensuring client safety, decreasing conception costs and reducing time-to-market are the three conflicting objectives at play when choosing and building processes for structural durability assessment. Requirements regarding the reliability of vehicle chassis parts seek to limit the probability (risk) of fatigue failure under regular (service) use cases over a given lifetime goal. Test conditions seek to validate such requirements when designing a new car model. They must be elaborated with respect to the uncertainties inherent to both fatigue failure, automotive industrial process and targeted customer uses (Johannesson (2014) Chap. 1). The choice of a design load must be accounted for. One method is to gather and compile real driving events, like in Standard Loading Histories (Berger et al. (2002) or Heuler and Klätschke (2005)).

When designing a part or organ, the chosen loading level must be proven representative of the whole population of in-service loads. Only thus can engineers control that the designed system's probability of facing failure in service lies below the maximum acceptable risk. This paradigm, opposed to maximalist design, aims to reduce costly system overdesigns (Svensson and Johannesson (2013)). Risk of failure of

*Corresponding author:
Email address: emilien.baroux@stellantis.com. (Emilien Baroux)

a part in service is usually worked out using a stress-strength interference approach (Lipson et al. (1967)). System failure ($S > R$) is associated to the idea that the load (Stress S) was too "severe" for the designed part, given its resistance (Strength R) to load level S. The historical approach (Thomas et al. (1999)) relies on the limitation that both S and R are described by a scalar variable called severity. This stiffens the versatility and robustness of our design models in our innovative and competitive industry. New car architectures (smart cars), power technologies (EV/HEV), assisted driving services (car vision) or new use paradigms (autonomous cars, carsharing) will modify the way cars are used and loaded in service, as well as the stiffnesses and weaknesses of their structure, constantly questioning design choices and models.

Following Genet (2006) and Eryilmaz (2011), one way to overcome the limitations of scalar severity lies in an enhanced description of the reliability of a complex structure submitted to multi-input mechanical loads. Our intention is to develop the questions surrounding the choice of design loads for reliability validation. We will explore this concept of "severity", lying in our definition of risk, by proposing a multivariate description of client loads and multiple pseudo-damage variables, both inspired of Johannesson (2014) Chap. 2 and 3.

We present a multidimensional damage characterization method applied to car chassis submitted to multi-input loads in Sec. 2. We propose a multivariate description of client loads in Sec. 3. In the same section, from a labelled client measurement campaign, we identify and quantify several different driver profiles in terms of induced damage. We then elaborate on the reconstruction of client loads from proving ground tracks in Sec. 4. From these discussions, we will develop questions and insights towards choosing design loads in the article perspectives, Sec. 5.

2. Fatigue pseudo-damage

2.1. Global loading histories

We restrict our study to the design of car chassis parts (wheel axles, rear and front suspensions) and their resistance to crack initiation and propagation under service mechanical loads on each wheel axle. These multi-entry variable amplitude loads should contain all the information we need to quantify induced fatigue, at each point of car chassis parts, by a car use. We denote any of such loading histories as

$$\vec{\mathbf{F}} = (\mathbf{F}_j)_{j\in\{1,n_F\}} \text{ where } \mathbf{F}_j = \Big[F_j(t), t \in [0,T]\Big] \text{ with } j = \{1 \text{ or } 2... \text{ or } 6;\ f \text{ or } r;\ l \text{ or } r\} \tag{1}$$

denoting f or r, l or r whether the effort (degrees of freedom 1 to 3) or moment (dof 4 to 6) is applied to the front or rear axles, on the left or right wheel (e.g. $F_{X,f,l}$), and n_F being the total number of load components. X, Y, Z directions are associated respectively to deceleration, lateral and vertical solicitations.

2.2. Damage from multiaxial local stress

Fracture at a material point M can be predicted by calculating a fatigue variable from its local stress history and comparing it to an adequate threshold. We denote $\Big[\underline{\underline{\sigma}}(M,t), t \in [0,T]\Big]$ the local stress history at point M, where $\underline{\underline{\sigma}}$ is the second-order Cauchy stress tensor. Under multiaxial cyclic loads, multiaxial fatigue criteria determine such a fatigue variable τ for each stress cycle. The choice of τ determines the chosen model of physical fatigue phenomena, see Weber (1999) Chap. 1 for different definitions of τ. Damage models for variable amplitude loads (our concern) are a generalization of these cyclic fatigue criteria and may exploit the same variable for fatigue prediction.

Methods based on Miner's Law (Miner (1945)) allow to linearly cumulate damage from loading samples. The most common signal decomposition technique used in cooperation with Miner's Law is the rainflow cycle counting method, see Rychlik (1987) for method generalities, and Pierron (2018) for an example of experimental verification. Regardless of the order of its extrema, the rainflow counting of a scalar signal $[\tau(M,t), t \in [0,T]]$ returns n_c rainflow cycles with amplitudes $(\Delta\tau)_i$ and means μ_i. Following the examples of Susmel and Lazzarin (2002) and Meggiolaro and de Castro (2012), marginal damage associated to each rainflow cycle of the fatigue variable τ is modeled using a Basquin model of a Wöhler curve: $S_0^\beta = N(\Delta\tau)^\beta$. This set of hypotheses leads to the following expression of local damage

$$D\left(M, \left[\underline{\underline{\sigma}}(t), t \in [0,T]\right]\right) = \sum_{i}^{n_c} \frac{(\Delta\tau)_i^{\beta(M)}}{S_0^{\beta}(M)} \tag{2}$$

2.3. Local stress on linear structures

We make the simplifying assumption that our structure's answer is quasi-static under service loads. It means that instantaneous local stress at each point of our structure depends only on instantaneous values of $\vec{\mathbf{F}}$. This quasi-static approximation is hindered by high frequency components such as pavements or large spectrum obstacles like sidewalks or potholes. Other fatigue characterization methods may take into account the effects of high frequency, see for instance Benasciutti et al. (2013).

We ignore the non-linear effects of elements like rubber joints or mechanical stops, on the structure's mechanical response. Local loads at each point of the structure are found using the principle of superposition

$$\underline{\underline{\sigma}}(M,t) = \sum_{j}^{n_F} \underline{\underline{K}}_{M,j} F_j(t) \tag{3}$$

denoting $\underline{\underline{K}}_{M,j}$ stress localization second-order tensors associated to each global load component.

We make the further assumption that the damage variable τ is a linear form $\tau = \underline{k}_f . \underline{\underline{\sigma}} . \underline{h}_f$. Such a property holds for damage variables like shear stress calculated on point M's critical slip plane. From Eqs. 2 and 3, damage at point M is

$$D(M, \vec{\mathbf{F}}) = \sum_{i}^{n_c} \frac{1}{S_0^{\beta}(M)} \left(\Delta \left(\sum_{j}^{n_F} \underline{k}_f . \underline{\underline{K}}_{M,j} . \underline{h}_f \mathbf{F}_j \right) \right)_i^{\beta(M)} \tag{4}$$

2.4. Pseudo-damage

Choosing an adequate norm $\|.\|$, let us rewrite

$$\frac{1}{S_0(M)} \sum_{j}^{n_F} \underline{k}_f . \underline{\underline{K}}_{M,j} . \underline{h}_f \mathbf{F}_j = \|\vec{A}_M\| \vec{e}_{A_M} . \vec{\mathbf{F}} \tag{5}$$

We propose to use the canonic 2-norm in space $\mathbb{R}^{n_F}$. The term $\|\vec{A}_M\|_2$ is akin to stress magnification level around the point M in the structure. It depends on the structure's rigidity, the point's location, its geometry and its stress intensity factors. The unit vector $\vec{e}_{A_M}$ stems from privileged crack microscopic initiation and propagation directions. Several points in a car chassis may have the same stress orientation $\vec{e}_{A_M}$.

Thanks to the linearity of rainflow counting, we can define pseudo-damage $\hat{D}_M(\mathbf{F})$ as

$$D(M, \vec{\mathbf{F}}) = \|\vec{A}_M\|_2^{\beta(M)} \sum_{i}^{n_c} \left(\Delta(\vec{e}_{A_M} . \vec{\mathbf{F}}) \right)_i^{\beta(M)} = \|\vec{A}_M\|_2^{\beta(M)} \hat{D}_M(\vec{e}_{A_M} . \vec{\mathbf{F}}) \tag{6}$$

Eq. 6 is a generalization of pseudo-damage calculated from uniaxial load signals, presented in Johannesson (2014) Chap. 3. In the rest of the article, this exponent will be considered to be unvariably equal to 4 for the weak points to be designed. It is a conventional value for the Basquin exponent of weld beams' fully reversed (R=-1) traction Wöhler curves. Therefore, we can rewrite $\hat{D}_M = \hat{D}$.

2.5. Chassis weak points and damages

Design experience helps to determine what kind of points one wants to design in a new car chassis. The structure directs stress directions around them. Local loading at these points can be associated to specific load cases, such as load cases presented in Fig. 1. Each load case's induced damage is preponderant for different sensible points in the structure. We can deduce a satisfying pseudo-damage characterization of all validation points on a car chassis by picking a set of complementary load cases.

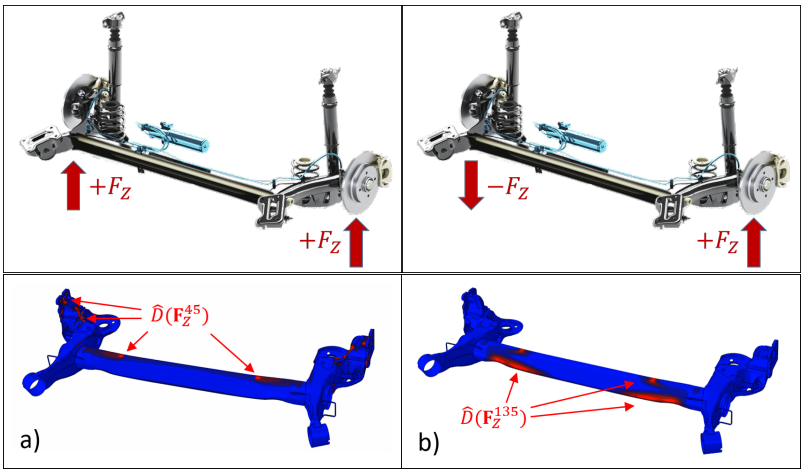

Fig. 1. Car rear cross member under symetric and asymetrical vertical loads, inspired from Happian-Smith (2002) and Genet (2006)

To illustrate this restriction in our article, we consider a few load cases, made from simple combinations of global load components, defined by

$$\mathbf{F}^{\gamma}_{X,f} = cos(\gamma)\mathbf{F}_{X,f,l} + sin(\gamma)\mathbf{F}_{X,f,r} \tag{7}$$

and likewise for directions Y and Z, denoting γ an angle of combination. For example, in Fig. 1 a), $\mathbf{F}^{45}_{Z,f}$, being the sum of front-wheel vertical efforts, corresponds to the bending loading case. A difference in vertical efforts causes both torsion and bending of the cross member and is represented by $\mathbf{F}^{135}_{Z,f}$, case b).

We consider that we want to design the weakest points under a number n_d of load cases created using Eq. 7. Let us define the pseudo-damage vector

$$\vec{\hat{D}}(\vec{\mathbf{F}}) = \left(\hat{D}(\mathbf{F}^{\gamma_k}_{j})\right)_{j\in\{1,n_d\}} \tag{8}$$

containing pseudo-damages from Eq. 6 calculated using a single constant Basquin exponent β and different indices j from Eq. 7. This pseudo-damage vector contains all the information we want to determine the load's induced damage.

2.6. On damage, load and severity

In the scalar case, damage and load descriptions were both scalar and simultaneously monotonous (see Bignonnet and Thomas (2001)). Scalar variables are always ordered: a load A is more severe than a load B if its description is higher than the other one. Severity was easily defined as an isomorphism of either damage or load descriptions.

Under multi-input loads, given several damage dimensions (that is, several different design points at the same time), damage and load description's dimensions are independent and stem from engineering decisions. Severity aims to compare loads to one another in terms of fatigue. We are unable to predict from equations and mechanics alone how severity could be defined mathematically. We have to dive deeper into the description of client uses to understand how severity arises from their diversity.

3. Measuring client damage

3.1. Client load description

In Sec. 2 we have described how to build pseudo-damage from any loading history on a car. We can apply this calculation to client loading histories. First, we need to be more precise on our definition of a client and of service loads.

A car service loading episode occurs while the car is used by a *specific driver*, over a *specific path*, with a given *payload* (passengers and luggage) at a given *time* in a given *region* with its corresponding driving legislation and cultural habits. The *structure* is therefore opposed to a specific trajectory and its mechanical answer loads the car chassis. This defines a single client use case.

Driver $\mathcal{D}$, *trip* $\mathcal{T}$ (path, road properties, legislation and traffic situations), *payload* $\mathcal{M}$ are the three variables that determine load over one use case (see Fig. 2). The customer load distribution is multivariate as per our model. We need to exploit different sources of information to characterize these three sources of variability.

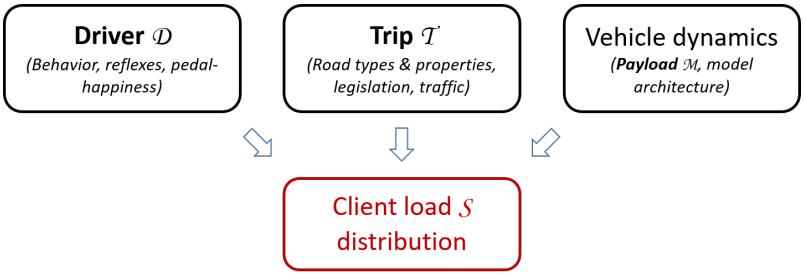

Fig. 2. Sources of variability in car service loadings (adapted from Johannesson (2014))

3.2. Client measurement campaign

To measure a population of target client uses, we can proceed using one of two types of sampling:

- Acquiring enough random samples to be representative of the whole population;
- A stratified selection procedure using labelled samples based on the decomposition in Fig. 2.

Developments to apply the former are presented in Chojnacki (2021). In this article, the second approach is preferred. To control the effects of each source of variability - driver, trip and payload - labelled campaigns may force some of these parameters. In our study, we use a specific kind of campaign in which we have fixed variables $\mathcal{T}$ and $\mathcal{M}$, called Fixed Trip & Payload India 2011 ($\mathcal{I}11$).

In the campaign $\mathcal{I}11$, 11 clients (C1 to C11) drove with the same vehicle on the same path, in India, one client per day for 11 days. Efforts applied to each wheel axle of the car were measured over a distance of 220km for each client (moments were not measured). Said loadings are denoted $\vec{\mathbf{C}}_c$ for $c \in \{1, 11\}$.

3.3. Client pseudo-damage

For the sake of illustration, we only keep the 6 efforts applied to the car's two front wheel axles. We calculate from them 12 scalar signal combinations $(\mathbf{F}_j)_{j\in\{1,n_d\}}$ using Eq. 7 over the 3 directions (X, Y, Z) with 4 angles of combination $\gamma \in (0, 45, 90, 135)$. Pseudo-damage was calculated using Eq. 6 with a Basquin exponent $\beta = 4$. The rainflow counting on each load combination was performed on MATLAB using the toolbox WAFO (Brodtkorb et al. (2000)) following the rules of ASTM E1049-85 (2017).

The Fig. 3 shows the values of pseudo-damage for a few outstanding clients and for each pseudo-damage component's mean. Each radius of this radar corresponds to one pseudo-damage component, individually centered and reduced. Each 120-degree sector corresponds to the 4 pseudo-damages calculated over one direction (X, Y, Z).

The larger circle in this figure shows an abstract client C_a whose pseudo-damages are equal to client mean plus three standard deviations s_j for all components. This client will be the example used in Sec. 4.4.

Clients C3, C5 and C9 stand out as dominating the rest of the campaign. We can see however that these clients can not be ordered over all components at once. It means that they gather and maximize pseudo-damage components respectively along the Z, X and Y directions. They induce more damage on the structure from combinations of vertical, deceleration or lateral loads, compared to the other clients.

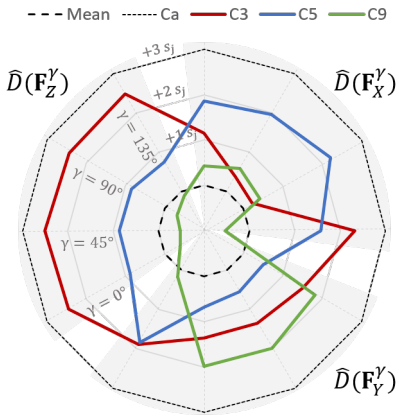

Fig. 3. Pseudo-damage dispersion over $\mathcal{I}11$ clients

This multidimensional description of client pseudo-damages helps us to compare clients on each component of the vector. In the next paragraph, we will apply variable reduction methods to achieve a simpler and sufficient description of client pseudo-damage vectors towards their statistical distribution.

3.4. Driving profile description

We perform a principal component analysis (PCA) to describe the variations of pseudo-damage vectors using fewer dimensions (Husson et al. (2011)). The principal components (PC) (or principal axes) are linear combinations of the pseudo-damages with maximum variance and are pairwise orthogonal. Here, the first three components express 97.9% of data variability, see Table 1.

The Table 1 also shows the correlation of each PC to the pseudo-damage's components. First component PC1 is positively correlated to all pseudo-damages. This is called the size effect: a client with a high (resp. low) coordinate on the PC1 axis has high (resp. low) pseudo-damages overall. The second component PC2 is positively correlated with the pseudo-damages induced from combinations of longitudinal and lateral loads, and negatively correlated with the vertical ones. The third component PC3 is positively correlated with the longitudinal pseudo-damages and negatively with the lateral ones.

Table 1. Principal component analysis: pseudo-damages correlations with the PCs.

	$\hat{D}(F_X^0)$	$\hat{D}(F_X^{90})$	$\hat{D}(F_Y^0)$	$\hat{D}(F_Y^{90})$	$\hat{D}(F_Z^0)$	$\hat{D}(F_Z^{90})$
Corr PC_1(76.6%)	9.30	7.80	8.50	8.30	9.10	9.20
Corr PC_2(13.8%)	2.20	4.00	3.70	4.20	-3.80	-3.70
Corr PC_3(7.6%)	2.80	4.80	-3.70	-3.60	-0.20	-0.50

A client clusterization (Husson et al. (2011)) reveals five clusters. The projection of the clusters on each PC allows us to describe them (see Fig. 4). The center $(0, 0)$ of the cloud corresponds to mean pseudo-damage behaviors. PC1 makes it possible to distinguish the clients according to their multiaxial pseudo-damages. The cluster 1 includes clients with significantly lower than mean pseudo-damages. The cluster 2 includes clients C4 and C6 having medium pseudo-damages. The remaining clusters singularize clients C3, C5 and C9.

We have explored the question of client damage description. As mentioned in the introduction, we want to question the choice of design loads from statistics on client loads. In the next section, we will discuss the reconstruction of one or a group of these clients from reference proving grounds to further feed this discussion.

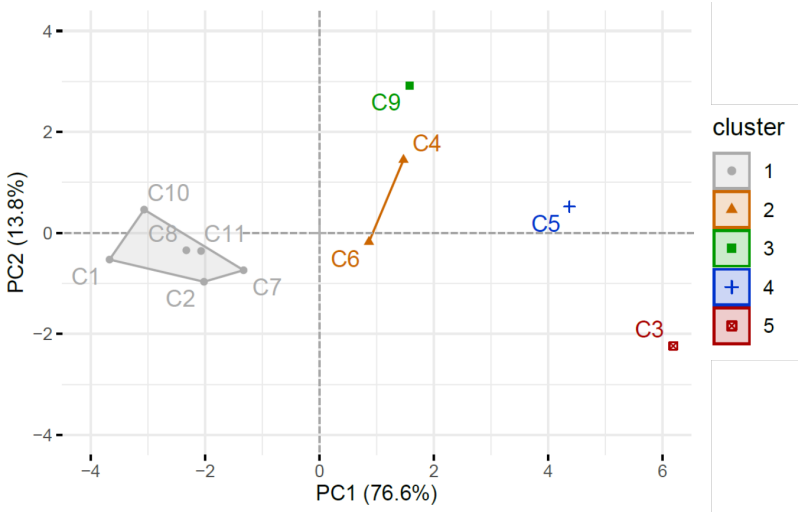

Fig. 4. PCA : clients scatterplot projection on plane PC1-PC2.

Table 2. Client characterization: the v-test is the value of the standardized difference between each cluster's mean and the overall mean: $|v| > 1.96$ indicates significant difference.

Client	Client C3				Client C5		Client C9	
Pseudo-damage	$\hat{D}(F_Y^0)$	$\hat{D}(F_Y^{90})$	$\hat{D}(F_Z^0)$	$\hat{D}(F_Z^{90})$	$\hat{D}(F_X^0)$	$\hat{D}(F_X^{90})$	$\hat{D}(F_Y^0)$	$\hat{D}(F_Y^{90})$
v-test	1.58	1.43	2.58	2.54	1.96	2.33	1.90	2.08

4. Client reconstruction from proving grounds

4.1. Proving grounds

We have argued that a choice of design loads should be achieved and justified from knowledge of client loads. Once this choice is made by load data engineers, a targeted load must be translated into a reconstructed, repeatable test signal. A generic method to derive simpler loads from complex ones is presented in Raoult and Delattre (2020). It uses damage equivalency in a damage reconstruction protocol. That method relies on measurements realized on a vehicle driving on tracks, constitutive of proving grounds.

Historically, proving ground tracks were reproduced from real-life driving events. These samples were kept as representative of damaging events in a car's life, and as relevant, by experience, to design reliable car structures. These events have controlled dimensions, they are repeatable and easily associated to real life situations. The obstacles met, the tested car's trajectory and the added mass are fixed. From Fig. 2, we can say that proving ground conditions set both Driver, Trip and Payload for all vehicle models.

In this study, we consider a reference set of tracks performed with the very same car of $\mathcal{I}11$. Their load components are the same as in Eq. 1. Among these tracks, labelled T1 to T5, we respectively find emergency braking, a sample of common driving events, potholes, pavements and short turns.

4.2. Track pseudo-damage

We can replicate our previous damage calculation on track loads T1 to T5 using Eq. 8. In order to compare, on the same radar, heterogeneous track pseudo-damages to the client ones of Fig. 3, we need to use the same graphical parameters and to inflate track pseudo-damages according to their duration.

The Fig. 5 b), c) and d) show the shapes of track pseudo-damage radars compared to our three severe clients C3, C5 and C9. Each of these track involves an arbitrary repetition of a single kind of events. Compared to real-life loads, they emphasize specific pseudo-damage components. But they allow the engineer to put an emphasis on distinct kind of solicitations, namely, vertical, deceleration or lateral efforts.

We also compare the client mean and tracks T1 and T2 in a). Tracks appear to be complementary in explaining client pseudo-damages.

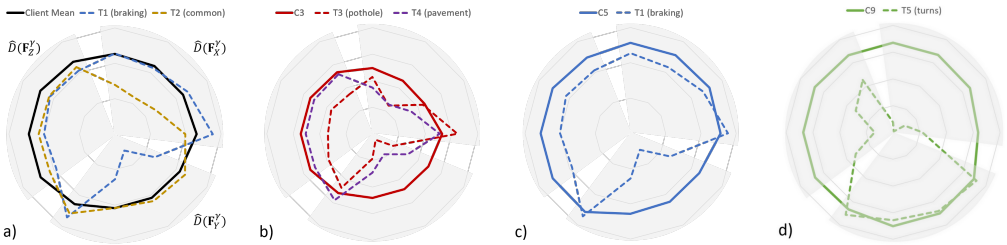

Fig. 5. Pseudo-damage shape comparison between tracks and: a) Client mean; b) Client C3; c) Client C5; d) Client C9

4.3. Construction of a target client from the customer base

We have seen from Sec. 3.4 that our client pseudo-damage population is heterogeneous. It is indeed composed of core and extreme clients, each displaying a different profile. We cannot yet provide a relevant representative client for our creation of a design load. In this section, we will simplify this problem and pick an illustrative client having fixed pseudo-damages accumulated over 220km. A justified choice will be presented in a later study. We choose a client load $\mathbf{C}_\alpha$, corresponding to a high quantile over all pseudo-damage components, defined as

$$P\left(\vec{\hat{D}}(\mathbf{C}) \succ \vec{\hat{D}}(\mathbf{C}_\alpha)\right) \leq \alpha \tag{9}$$

where $\vec{u} \succ \vec{v}$ implies that each component of $\vec{u}$ is greater than the corresponding one in $\vec{v}$. $\mathbf{C}$ is a random outcome from our client load population. This target client is a generalization of an α-quantile of a scalar random variable.

If client pseudo-damage vectors are issued from a gaussian random variable, this target load's damage is

$$\vec{\hat{D}}(\mathbf{C}_\alpha) = \begin{pmatrix} \mu_X^0 + z_{1-\alpha} s_X^0 \\ \dots \\ \mu_Z^{135} + z_{1-\alpha} s_Z^{135} \end{pmatrix} \tag{10}$$

denoting μ_X^γ and s_X^γ respectively the mean and standard deviation of pseudo-damage values $\hat{D}(\vec{\mathbf{F}}_X^\gamma)$ over our clients from $\mathcal{I}11$, and same for Y and Z. And $z_{1-\alpha}$ is the $(1-\alpha)$-quantile of a standard normal distribution. If $\alpha = 1\%$, $z_{1-\alpha} \approx 3$ and C_a used in Fig. 3 verifies $\vec{\hat{D}}(\mathbf{C}_\alpha) = \vec{\hat{D}}(\mathbf{C}_a)$

4.4. Reconstruction of a target client from the proving grounds

To reconstruct the pseudo-damages associated to client C_a, we look for a loading history composed of a chaotic sequence of repetitions of tracks T1 to T5, inducing equivalent damage.

Using rainflow counting in Eq. 2 makes the order of concatenation irrelevant to damage calculation. However, damage obtained from a rainflow counting on a chaotic concatenation of single loads is not equal to the sum of damages calculated from rainflow countings on the single loads. Indeed, damage quantification from rainflow counting is dependent on the processing of the rainflow residual terms (Marsh et al. (2016)). Nevertheless, we make the hypothesis that the damage of a load $\mathbf{C}_{\vec{n}}$ constructed from n_e repetitions of each track T_e is the sum of the damages calculated from each track. The induced pseudo-damage is then

$$\vec{\hat{D}}(\mathbf{C}_{\vec{n}}) = \sum_{e=1}^{5} n_e \vec{\hat{D}}(\mathbf{T}_e) \tag{11}$$

We look for $\mathbf{C}_{\vec{n}}$ as close as possible to our target client in terms of induced pseudo-damage. We want to solve the following constrained quadratic optimization

$$\min_{\vec{n}} \|\vec{\tilde{D}}(\mathbf{C}_{\vec{n}}) - \vec{\tilde{D}}(\mathbf{C}_a))\|_2^2 \quad \text{with} \quad \vec{n} \succ \vec{0} \tag{12}$$

We used here a canonic 2-norm on space $\mathbb{R}^{n_d}$. Otherwise, a weighted norm would allow us to focus on the precise reconstruction of specific pseudo-damage components. This choice may be motivated by the diversity of driver profiles and its consequence on the variability of each pseudo-damage component. It may also be motivated by the importance of each pseudo-damage component when it comes to designing vehicle parts. The choice of the minimization criterion can be tricky, and a further study will be exclusively dedicated to the search of equivalent loads towards the creation of design loads.

Table 3 shows the results of a constrained quadratic optimization on this problem using a global search with default parameters from the R package QUADPROG (Goldfarb and Idnani (1983)).

Table 3. Optimal 2-norm mix of tracks to reconstruct client C_a

	T1	T2	T3	T4	T5
Obstacle type	Braking	Common driving	Pothole	Pavement	Turns
Optimal combination	176	11	0	0	2

Here only three tracks have been retained. Tracks are characterized as $\mathbb{R}^{12}$ damage vectors, and they might be redundant if one track pseudo-damage vector can be reconstructed from a combination of other ones. The completeness of a set of tracks will be discussed in a further study. Beside, we did not compute a relevant score to judge our reconstructed load. The algorithm's stopping criterion depends on the chosen norm and on the convexity of our research space.

5. Conclusion and perspectives

In order to reliably design a car chassis, we need to characterize the fatigue induced by service loads and to determine load conditions and levels that are representative of client uses. We have introduced a vectorial description of the fatigue induced by multi-input variable amplitude loading histories on car chassis parts. A further investigation should assess the prediction performances of our pseudo-damage characterization.

We have proposed a method to link weak points in our structure to specific pseudo-damage components derived from global structural load cases. The choice of a set of such load cases must be motivated by previous validation processes and experience.

Then, the variability of car loads in service was developed into a multivariate description of client profiles. We distinguish the effects of the driver, the trip and the vehicle's dynamics. Thus, we have proposed a method to acquire statistical knowledge on the distribution of client loads using labelled measurement campaigns.

From an example of such a campaign ($\mathcal{I}11$), we have evaluated the effect of one source of variability: the driver's behavior. Using principal component analysis, we have found that the effect of the variable Driver on induced damage can be described using a little number of variables. We have proposed an interpretation of these variables by referring to simple load cases. The definitions and variety of trips and payloads over car use cases, as well as the extrapolation from client samples to whole car lives, will be investigated in a further study, compiling different campaigns. Thanks to innovations in sensor integration and Big Data methods (Chojnacki (2021)), small-cost integration of measurement sensors and post-processing routines becomes achievable in connected vehicles. A larger anonymous survey of client loads and uses will increase the precision of our knowledge of client uses.

We also have isolated extreme client uses in our campaign $\mathcal{I}11$ through client clustering. Pending the further analysis of larger databases using extreme value statistics, we can only draw partial conclusions on the distribution of all driver profiles over our client population. The existence and the specificity of prominent driver profiles raise however the question of the desired representativeness of the design load (Rockafellar and Royset (2015)). Its choice must account for the likelihood of all accepted uses in what we have classified as service uses.

Finally, we have proposed, for a given abstract client pseudo-damage vector, a method to reconstruct it using simple and controlled track loads. The results obviously depend on the parameters and criteria used in the optimization. Using track samples to elaborate test conditions has the advantage of managing realistic and reproducible car loads, in accord with current customs in the automotive industry. We have raised the questions of representativeness and redundancy of a set of tracks with respect to the variety of clients. This comforts us towards handling a growing set of available tracks to build physical design loads.

We have argued that design conditions need to be representative of the whole population of service uses. However, they must also be appropriate with respect to the definition of risk in project requirements to fully adapt the SSI method to our validation needs.

References

ASTM E1049-85(2017), 2017. Standard Practices for Cycle Counting in Fatigue Analysis. Standard. ASTM International. West Conshohocken, PA.

Benasciutti, D., Cristofori, A., Tovo, R., 2013. Analogies between spectral methods and multiaxial criteria in fatigue damage evaluation. Probabilistic Engineering Mechanics 31, 39–45.

Berger, C., Eulitz, K.G., Heuler, P., Kotta, K.L., Naundorf, H., Schuetz, W., Sonsino, C.M., Wimmer, A., Zenner, H., 2002. Betriebsfestigkeit in germany - an overview. International Journal of Fatigue 24, 603–625.

Bignonnet, A., Thomas, J.J., 2001. Fatigue assessment and reliability in automotive design, in: SAE Brasil International Conference on Fatigue, SAE International.

Brodtkorb, P., Johannesson, P., Lindgren, G., Rychlik, I., Rydén, J., Sjö, E., 2000. WAFO - a Matlab toolbox for the analysis of random waves and loads, in: Proc. 10th Int. Offshore and Polar Eng. Conf., ISOPE, Seattle, USA, pp. 343–350.

Chojnacki, D., 2021. Towards a better understanding of mechanical stress applied by passenger vehicle customers with optimized instrumentation and relevant data post-processing methodologies, in: Fatigue Design Proceedings 2021.

Eryilmaz, S., 2011. A new perspective to stress–strength models. Annals of the Institute of Statistical Mathematics 63, 101–115.

Genet, G., 2006. A statistical approach to multi-input equivalent fatigue loads for the durability of automotive structures. Ph.D. thesis. Chalmers University of Technology and Göteborg University.

Goldfarb, D., Idnani, A., 1983. A numerically stable dual method for solving strictly convex quadratic programs. Mathematical Programming 27, 1–33.

Happian-Smith, J. (Ed.), 2002. An Introduction to Modern Vehicle Design. Butterworth Heinemann.

Heuler, P., Klätschke, H., 2005. Generation and use of standardised load spectra and load-time histories. International Journal of Fatigue 27, 976–990.

Husson, F., Lê, S., Pagès, J., 2011. Exploratory multivariate analysis by example using R. volume 15. CRC press Boca Raton.

Johannesson, P. & Speckert, M. (Ed.), 2014. Guide to load analysis for durability in vehicle engineering. John Wiley & Sons, Ltd.

Lipson, C., Sheth, N.J., Disney, R.L., 1967. Reliability prediction - Mechanical stress/strength interference. Technical Report. University of Michigan.

Marsh, G., Wignall, C., Thies, P.R., Barltrop, N., Incecik, A., Venugopal, V., Johanning, L., 2016. Review and application of rainflow residue processing techniques for accurate fatigue damage estimation. International Journal of Fatigue 82, 757–765.

Meggiolaro, M.A., de Castro, J.T.P., 2012. An improved multiaxial rainflow algorithm for non-proportional stress or strain histories – part ii: The modified wang–brown method. International Journal of Fatigue 42, 194–206.

Miner, M.A., 1945. Cumulative damage in fatigue. Journal of Applied Mechanics 3, 159–164.

Pierron, Q., 2018. Caractérisation de la fatigue des assemblages soudés soumis à des chargements à amplitude variable. Ph.D. thesis.

Raoult, I., Delattre, B., 2020. Equivalent fatigue load approach for fatigue design of uncertain structures. International Journal of Fatigue .

Rockafellar, R.T., Royset, J.O., 2015. Engineering decisions under risk averseness. ASCE-ASME Journal of Risk and Uncertainty in Engineering Systems, Part A: Civil Engineering 1.

Rychlik, I., 1987. A new definition of the rainflow cycle counting method. International Journal of Fatigue 9, 119–121.

Susmel, L., Lazzarin, P., 2002. A bi-parametric wöhler curve for high cycle multiaxial fatigue assessment. Fatigue and Fracture of Engineering Materials and Structures 25, 63–78.

Svensson, T., Johannesson, P., 2013. Reliable fatigue design, by rigid rules, by magic or by enlightened engineering. Procedia Engineering 66, 12–25.

Thomas, J., Perroud, G., Bignonnet, A., Monnet, D., 1999. Fatigue design and reliability in the automotive industry, in: Marquis, G., Solin, J. (Eds.), Fatigue Design and Reliability. Elsevier. volume 23 of *European Structural Integrity Society*, pp. 1–11.

Weber, B., 1999. Fatigue multiaxiale des structures industrielles sous chargement quelconque. Ph.D. thesis. Institut National des Sciences Appliquées de Lyon.